Sustainable Marine Structures
https://journals.nasspublishing.com/index.php/sms

ARTICLE

Numerical Simulations of the Pitching Airfoil by Using Discrete Vortex Method

Peng Ren[1,2] Ke Lin[1,2] Jiasong Wang[1,2,3*]

1. Department of Engineering Mechanics, School of Naval Architecture, Ocean and Civil Engineering, Shanghai Jiao Tong University, Shanghai, 200030, China
2. Key laboratory of Hydrodynamics (Ministry of Education), Shanghai Jiao Tong University, Shanghai, 200030, China
3. SJTU-Sanya Yazhou Bay Institute of Deepsea Science and Technology, Sanya, Hainan, 572024, China

ARTICLE INFO

Article history
Received: 5 September 2023
Revised: 15 October 2023
Accepted: 25 October 2023
Published Online: 31 October 2023

Keywords:
Discrete vortex method
Pitching motion
Airfoil
Thrust

ABSTRACT

This paper presents a two-dimensional discrete vortex method that uses the vortex growing core model to simulate the unsteady force and the wake patterns of the pure pitching airfoil efficiently and accurately. To avoid the random fluctuation caused by the random walk method, a vortex growing core method is used to simulate the viscous diffusion motion. In addition, the vortices fall off randomly on the body surface. Referring to the experimental configurations of Mackowski and Williamson (2015), a good agreement is achieved through the comparisons between the present simulation results and the experimental results, including the mean force coefficients, oscillation amplitude and wake patterns. It shows that the two-dimensional discrete vortex method can be used to predict the mechanical behavior and wake patterns on the pitching airfoil motion.

1. Introduction

Birds, as well as some marine creatures, use vibrations of their wings, fins or other parts to generate thrust and lift. From the perspective of bionics, some scholars have focused on creating thrust-generating devices, just like autonomous underwater vehicles and some flapping wing micro-aerial vehicles [1-3]. This kind of device is different from the turbines which rotate around an external axis to achieve electricity generation [4-6], but to control the

*Corresponding Author:
Jiasong Wang,
Department of Engineering Mechanics, School of Naval Architecture, Ocean and Civil Engineering, Shanghai Jiao Tong University, Shanghai, 200030, China; Key laboratory of Hydrodynamics (Ministry of Education), Shanghai Jiao Tong University, Shanghai, 200030, China; SJTU-Sanya Yazhou Bay Institute of Deepsea Science and Technology, Sanya, Hainan, 572024, China;
Email: jswang@sjtu.edu.cn

DOI: http://dx.doi.org/10.36956/sms.v5i2.944

airfoil motion actively for realizing the bionic behavior such as propulsion, hovering, heaving and so on. In recent decades, more and more scholars focused on the thrust and lift generation mechanism of flapping wings and how this mechanism is influenced by various factors. The pure pitching motion of the airfoil simplifies the complex motion of the flapping airfoil, and the study by considering only the pitching motion is instructive for researchers to understand the evolution law of unsteady forces during the movement of the airfoil.

On the basis of Theodore's pioneer study [7] on the unsteady force of oscillating airfoil, Garrick [8] theoretically calculated the unsteady force caused by the pitching and heaving motion of the airfoil. The results showed that the pitching motion need high enough frequency to make the transition from drag to thrust, whereas the heaving motion could produce thrust at any frequency. Koochesfahani [9] visualized the wake structure of the pitching NACA 0012 and found that the wake structure can be modified by the control of the amplitude, frequency and shape of the vibration waveform. Further, Bohl and Koochesfahani [10] improved the experiment and introduced the method of estimating the mean force on the airfoil by using the measured mean and fluctuating velocity fields. Godoy-Diana et al. [11] captured the transition of the vortex streets in the wake flow of pitching airfoil from the Benard-von Karman (Bvk) wake to the reverse Bvk vortex street. The results also showed that this transition precedes the actual drag-thrust transition. Schnipper et al. [12] visualized a variety of wakes in a vertical soap film and mapped out the wake types in a phase diagram.

Similarly, some scholars used numerical simulation to discover the mystery of the pitching airfoil. Young and Lai [13] used a compressible two-dimensional Navier-Stokes solver to study the flow over a NACA 0012 airfoil which oscillated sinusoidally in the plunge. Chandravanshi et al. [14] used both a gridless Lagrange technique and a finite volume based Navier-Stokes solver to study the pure plunging motion of the airfoil. Wu et al. [15] studied the NACA 66 hydrofoil's pitching motion under the Lagrange coherent structures. In this study, he used the $k-\omega$ shear stress transport turbulence model coupled with a two-equation $\gamma - Re_\theta$ transition model for the turbulence closure was used. As a meshless numerical simulation method of Lagrange, the discrete vortex method has higher efficiency than the traditional CFD method. Therefore, some scholars also use the discrete vortex method to calculate the unsteady force and the wake structure of the pitching airfoil [16-19]. However, most of them used the method of random walk which was introduced by Chorin [20] to model the viscous diffusion and this method may cause the random fluctuation of order $Re^{-1/2}$ to the simulation result. To avoid this random fluctuation, some scholars used the growing core method [21-23] instead of the random walk method which was introduced by Park [24] in 1989. Also, some scholars specified the control layer thickness in advance according to the results of a trial and error procedure when using the discrete vortex method.

This study introduces a two-dimensional discrete vortex method to simulate the propulsive performance of the pitching airfoil. This method uses the vortex growing core method to simulate the viscous diffusion motion, instead of the random walk method. In addition, the vortices fall off randomly in this study instead of setting a fixed boundary layer thickness in advance. In order to validate the reliability of this method, the pure pitching motion of the airfoil referring to the experiment of Mackowski and Williamson [25] is simulated. For verifying the calculated results, the mean force coefficients, oscillation amplitude and wake patterns are compared.

In this paper, Section 1 introduces the background of the pitching airfoil and the research status of other scholars; Section 2 introduces the numerical implementation method for calculating the pitching airfoil; Section 3 shows the comparison between the simulation results and the experimental results; Section 4 draws a conclusion.

2. Numerical Method

2.1 Governing Equation

With the assumption of mass-force ignored, for the two-dimensional, incompressible, viscous flow, the fluid continuity equation and the Navier Stokes equation can be written as:

$$\nabla \cdot \boldsymbol{V} = 0 \tag{1}$$

$$\frac{\partial \boldsymbol{V}}{\partial t} + \boldsymbol{V} \cdot \nabla \boldsymbol{V} = -\frac{1}{\rho}\nabla p + \nu \nabla^2 \boldsymbol{V} \tag{2}$$

where $\boldsymbol{V}$ is the local velocity vector of the fluid, p is the pressure, ρ and ν are the uniform density and the kinematic viscosity, respectively. Taken the curl of the velocity on both sides of N-S equation, it can be written as:

$$\frac{\partial \omega}{\partial t} + \boldsymbol{V} \cdot \nabla \omega = \nu \nabla^2 \omega \tag{3}$$

where ω is the vorticity, $\omega = \nabla \times \boldsymbol{V}$. Considering the two-dimensional fluid, the continuity equation can be rewritten by introducing the stream function φ in the form of Poisson equation:

$$\omega = -\nabla^2 \varphi \tag{4}$$

To solve the equation, Chorin [20] introduced the operator splitting method which divided the equation into two

parts: the convection part and the viscous diffusion part.

$$\frac{\partial \omega}{\partial t} = -\boldsymbol{V} \cdot \nabla \omega \tag{5}$$

$$\frac{\partial \omega}{\partial t} = \nu \nabla^2 \omega \tag{6}$$

The convection equation indicates the invariance of the vorticity of the vortex elements when the vorticity field is discretized. For solving the convection equation, the Biot-Savart law can be used to obtain the summation speed of the vortex elements which concludes the velocity induced by the other vortices in the vorticity field and the incoming flow.

$$\boldsymbol{V}(\boldsymbol{r},t) = \boldsymbol{U}_\infty - \frac{1}{2\pi}\int \frac{(\boldsymbol{r}-\boldsymbol{r}_l)\times \omega(\boldsymbol{r}_l,t)}{(\boldsymbol{r}-\boldsymbol{r}_l)^2} dV \tag{7}$$

where $\boldsymbol{U}_\infty$ is the free stream incoming flow, $\boldsymbol{r}_i = (x_i, y_i)$ is the position vector of the i-th vortex element, $\omega(\boldsymbol{r}_i, t)$ is the vorticity of the i-th vortex element at $\boldsymbol{r}_i$. Since the solution of the equation exists singularity which will cause the calculated speed become infinite near the vortex element position, Chorin [20] introduced a vortex core model 'vortex-blob' which gave the vortex elements finite core radius to make the function bounded. Using this vortex core model, the equation can be rewritten discretely as [20]:

$$\boldsymbol{V}(\boldsymbol{r},t) = \boldsymbol{U}_\infty - \frac{1}{2\pi}\sum_{i=1}^{N} \Gamma_i \frac{(\boldsymbol{r}-\boldsymbol{r}_i)}{(\boldsymbol{r}-\boldsymbol{r}_i)^2 + \sigma_i^2} \tag{8}$$

where σ_i is the radius of the i-th vortex blob, Γ_i is the circulation of i-th vortex blob.

2.2 Numerical Implement of Pitching Airfoil

The stream function of the velocity induced by the i-th vortex element can be written as:

$$\varphi_i = -\frac{\Gamma_i}{4\pi}\ln(\boldsymbol{r}_i^2 + \sigma_i^2) \tag{9}$$

In the vorticity field, the total stream function of the j-th element can be written as:

$$\varphi_j = \boldsymbol{U}_\infty y_j - \sum_{i=1}^{N_s}\frac{\Gamma_i}{4\pi}\ln((\boldsymbol{r}_j-\boldsymbol{r}_i)^2+\sigma_i^2) - \sum_{k=1}^{N_w}\frac{\Gamma_k}{4\pi}\ln((\boldsymbol{r}_j-\boldsymbol{r}_k)^2+\sigma_k^2) \tag{10}$$

where N_s and N_w are the number of vortex elements generated in the surface and the vortex elements moving into the wake flow, respectively.

It should be noted that the no-slip condition and no-penetration condition should be satisfied near the solid body surface, which can be written as:

$$\begin{cases} \boldsymbol{u}\cdot\boldsymbol{s} = \boldsymbol{u}_b \cdot \boldsymbol{s} \\ \boldsymbol{u}\cdot\boldsymbol{n} = \boldsymbol{u}_b \cdot \boldsymbol{n} \end{cases} \tag{11}$$

where $\boldsymbol{s}$ and $\boldsymbol{n}$ are the tangent and normal vector of the solid body surface, respectively, $\boldsymbol{u}$ and $\boldsymbol{u}_b$ are the velocity of fluid near the solid body surface and the velocity of the body, respectively. Results from Qian and Vezza [26], Clarke and Tutty [27] and Wang and Yeung [28] have shown that no-slip condition and no-penetration condition are equivalent to determine the vorticity boundary condition. Therefore, satisfying either no-slip condition or no-penetration condition can uniquely determine the vorticity distribution.

As mentioned before, by solving the equation that satisfies the no-penetration condition, the vorticity distribution can be obtained on the solid body surface. This equation is calculated by differentiating the stream function of two adjacent control points on the surface, as written below.

$$\varphi_{i+1} - \varphi_i = \boldsymbol{U}_{ci} \cdot \boldsymbol{n} \Delta S_i \tag{12}$$

where φ_i is the stream function of the i-th control point on the surface, $\boldsymbol{U}_{ci}$ is the solid body surface velocity at the i-th control point, ΔS_i is the distance between i-th and (i+1)-th control points. As shown in Figure 1, N_s vortex elements are generated corresponding to N_s control points on the airfoil surface at each time step. For each two adjacent vortex elements, the corresponding equation to solve the vorticity of every newly generated vortex element. The form of the linear equations listed can be written as:

$$\boldsymbol{A}\Gamma = \boldsymbol{B} \tag{13}$$

where $\boldsymbol{A}$ is a $N_s \times N_s$ coefficient matrix, Γ is the vector composed of the vorticity of new vortexes, $\boldsymbol{B}$ is a vector. The elements of matrix $\boldsymbol{A}$ and vector $\boldsymbol{B}$ can be written as:

$$a_{ki} = \frac{1}{4\pi}\ln\frac{\left[(\boldsymbol{r}_{k+1}-\boldsymbol{r}_i)^2+\sigma_{i^2}\right]}{\left[(\boldsymbol{r}_k-\boldsymbol{r}_i)^2+\sigma_{i^2}\right]} \tag{14}$$

$$b_k = (\boldsymbol{U}_\infty - \boldsymbol{U}_{ck})(\boldsymbol{r}_{k+1}-\boldsymbol{r}_k) - \frac{1}{4\pi}\sum_{i=1}^{N_w}\Gamma_i \ln\frac{\left[(\boldsymbol{r}_{k+1}-\boldsymbol{r}_i)^2+\sigma_{i^2}\right]}{\left[(\boldsymbol{r}_k-\boldsymbol{r}_i)^2+\sigma_{i^2}\right]} \tag{15}$$

To ensure the conservation of the total vorticity in the field, the vorticity of the new elements and the vortex elements in the wake flow should satisfy the condition of the equation.

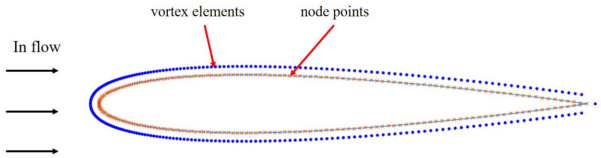

Figure 1. Scheme of the airfoil body surface and corresponding vortex elements.

$$\sum_{i=1}^{N_s}\Gamma_i = -\sum_{j=1}^{N_w}\Gamma_j \tag{16}$$

The vorticity of the newly generated vortex elements

can be solved. Under the circumstance of N_s unknowns and N_s + 1 equations, Walther [29] used the least square method and the Gauss elimination algorithm to solve this equation set. So far, the vorticity of newly generated vortex elements can be obtained by solving the convection equation, and the induced velocity between elements can be further calculated to update the whole field.

In addition, the solution of the viscous diffusion equation is the Green function. Usually, scholars use the random walk method which was introduced by Chorin to simulate the viscous diffusion motion. In order to avoid the random fluctuation caused by this method, Park [24] introduced a vortex growing core method, in which the growing radius of the vortex can be written as:

$$\sigma^{n+1} = \sqrt{\left(\sigma^n\right)^2 + 4.946 v \Delta t} \tag{17}$$

where σ^n and σ^{n+1} are the core radius at the n-th time step and the (n+1)-th step, respectively, Δt is the length of time step. Since then, both the convection part and the viscous diffusion part can be calculated, so that the whole vorticity field can be calculated by updating the vortex motion information.

Since at each time step, certain number of vortex elements are generated on the body surface, a total number of vortex elements will increase rapidly and then make the computational cost increase dramatically. Spalart [30] introduced a vortex element emergence method to control the total number of vortex elements in the whole field. At each time step, if two vortex elements satisfy the condition of the equation, merge these two vortex elements [30].

$$\frac{\left|\Gamma_i \Gamma_j\right|}{\left|\Gamma_i + \Gamma_j\right|} \cdot \frac{\left|\boldsymbol{r}_i - \boldsymbol{r}_j\right|^2}{(D_0 + d_i)^{3/2}(D_0 + d_j)^{3/2}} \le V_0 \tag{18}$$

where r_i and r_j are the position information of the i-th and the j-th vortex element, respectively, D_0 and V_0 are the governing parameters, d_i and d_j are the distance from the i-th and the j-th vortex element to the body surface, respectively. The vortex element information after the emergence is written as:

$$\boldsymbol{r} = \frac{\boldsymbol{r}_i \Gamma_i + \boldsymbol{r}_j \Gamma_j}{\Gamma_i + \Gamma_j} \tag{19}$$

$$\Gamma = \Gamma_i + \Gamma_j \tag{20}$$

2.3 Solution of Pitching Airfoil in Water Environment

This study uses the two-dimensional discrete vortex method introduced above to simulate the flow field and the mechanical behavior of the airfoil when the airfoil performs a pure pitch motion. The motion pattern of the airfoil shown in Figure 2 is considered, in which the airfoil oscillates around its quarter-chord point with the frequency f and the angle θ_0. The free stream flow direction is from the left to the right. At each time step, the angle of attack is controlled by a sinusoidal oscillation shown in the equation. Also, this study uses the reduced pitching frequency k which is nondimensionalized by the freestream velocity $\boldsymbol{U}_\infty$, the chord length c and the frequency f. The equation can be written as:

$$\theta = \theta_0 \sin(2\pi f t) \tag{21}$$

$$k = \frac{\pi f c}{U_\infty} \tag{22}$$

Another parameter charactering the pitching motion of the airfoil is the Strouhal number St_A. It can be defined based on the wake width A. In nature, swimmers and birds typically keep the St_A between 0.2 and 0.4 [31]. Due to the fact that the wake width A is difficult to measure, it can be replaced by the amplitude change of the airfoil's trailing edge [25].

$$St_A = \frac{fA}{U_\infty} = \frac{f \cdot 2c \cdot r_p \cdot \sin\theta_0}{U_\infty} \tag{23}$$

where r_p is the dimensionless length from the pivot point to the trailing edge (in this study, r_p = 0.75). Similarly, the Reynolds number which combines the free stream velocity, kinematic viscosity and the chord length is also one of the dominant parameters in the research of pitching airfoils. The Reynolds number can be defined as:

$$\mathrm{Re} = \frac{U_\infty \cdot c}{\upsilon} \tag{24}$$

In this study, the time step Δt is determined by a non-dimensional time step dt based on the free stream incoming flow velocity U_∞ and the chord length c, which can be seen in:

$$\Delta t = \frac{dt \cdot c}{U_\infty} \tag{25}$$

In this study, dt is set as 0.01 after some trial and error.

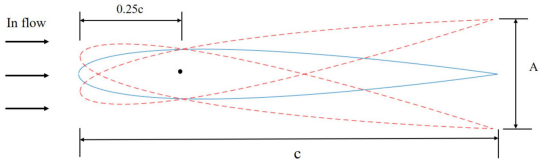

Figure 2. Geometry and kinematics of the airfoil.

The force exerted on the airfoil can be determined by the pressure distribution on the body surface. The tangential pressure gradient on the body surface can be written as [16]:

$$\frac{1}{\rho}\frac{\partial p}{\partial \boldsymbol{s}} = -\boldsymbol{s}\cdot a_c - \boldsymbol{n}\cdot\boldsymbol{r}\cdot\frac{d\omega}{dt} + \boldsymbol{s}\cdot\boldsymbol{r}\cdot\omega^2 + \nu\frac{\partial \Gamma}{\partial \boldsymbol{n}} \tag{26}$$

where $\boldsymbol{s}$ and $\boldsymbol{n}$ are the tangential and normal unit vector at the considering control point, respectively, $\boldsymbol{r}$ is the vector which starts from the pivot point to the considering control point, ω is the angular velocity at this control point t, p and a_c are the pressure and the acceleration on the selected control point, respectively. The first three terms of the right side in the equation represent the motion acceleration, rotational acceleration and centripetal acceleration, respectively.

By integrating circumferentially the body surface pressure, the streamwise force and the transverse force can be obtained. The form of thrust and lift coefficient can be written as equation (27) and equation (28), where the thrust coefficient C_T describes the propulsion performance of the pitching airfoil.

$$C_T = \frac{F_x}{\frac{1}{2}\rho U_\infty{}^2 c} \tag{27}$$

$$C_Y = \frac{F_y}{\frac{1}{2}\rho U_\infty{}^2 c} \tag{28}$$

3. Results and Discussion

For validating the computational accuracy of the two-dimensional discrete vortex method introduced above, this study carried out the numerical simulation of the pitching airfoil referring to the experimental configuration of Mackowski and Williamson [25]. The main parameters of the pitching airfoil are listed in Table 1. In Mackowski and Williamson's research, they studied the trends in propulsive performance with the flapping frequency, pitching angle and Reynolds number for NACA 0012. They also examined the unsteady forces on the pure pitching airfoil.

Table 1. Main parameters of the airfoil in the configuration of Mackowski and Williamson.

Airfoil Type	NACA 0012 Hydrofoil
Chord length	10 cm
Pivot location	0.25c
Reynolds number	12000, 16600
Pitching angle	2°, 4°, 8°, 16°, 32°
Reduced frequency range	0.5-12

Figure 3 shows the experimental and computational time average values of thrust coefficient C_T under the circumstance of Re = 12000, θ_0 = 2°, with the range of reduced pitching frequency k from 0.5 to 12. When the frequency is small, the value of the thrust coefficient is about –0.03, which is close to the static drag for the airfoil at zero angle of attack [32]. The thrust coefficient monotonically increases with the increase of the frequency k, and the transition from drag ($C_T < 0$) to thrust ($C_T > 0$) occurs at k = *10*. At k = *12*, C_T reaches the maximum of 0.02. Comparing the black points of the experimental results with the red points of the numerical results, it can be observed that the numerical results agree reasonably well with the experimental results in the whole range. In this case, the average thrust coefficient C_T and its variation trend can be calculated well.

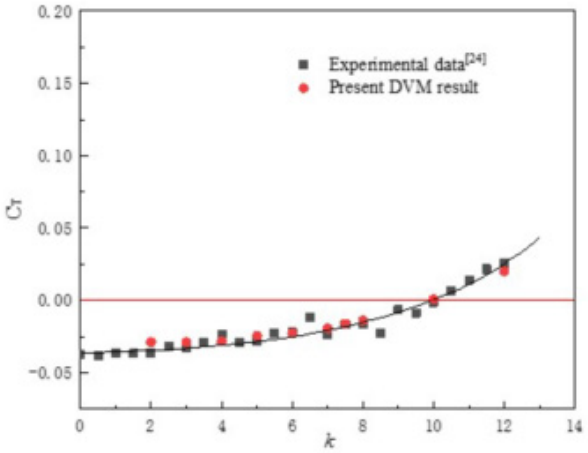

Figure 3. Experimental and computational values of thrust coefficient for the pitching NACA 0012 airfoil when Re = 12000, θ_0 = 2°.

As can be seen in Figure 3, both experimental and simulation results show that the crossover point between thrust and drag occurs at the position of k = 10 under the condition of Re = 12000, θ_0 = 2°. Further, Figure 4 indicates the crossover value of the reduced frequency k in the Reynolds number range from 1×10^4 to 3×10^4. Although there is a slight gap between the experimental and calculated values with the Reynolds number increasing, the overall trend shows great consistency. The crossover point decreases monotonically with the increase of the Reynolds number, which means that the higher Reynolds number makes it easier to generate thrust due to the airfoil pitching motion.

Figure 5 shows the variation trend between the mean thrust coefficient C_T and Strouhal number St_A at different pitching angles under the condition of Re = 16600. The black line is a curve fitted to the data. It can be observed that the mean thrust coefficient C_T and the Strouhal number St_A show a monotonically consistent increase when the pitching angle $\theta_0 \leq 8°$. However, this trend changes dramatically at the pitching angle of θ_0 = 16° and θ_0 = 32°. It can be observed that within the increasing frequency in large-amplitude cases, the thrust coefficients present a

decreasing trend instead of an increasing trend. Therefore, it is necessary to avoid the excessive pitching angle in the design of the pitching airfoil propulsion procedure.

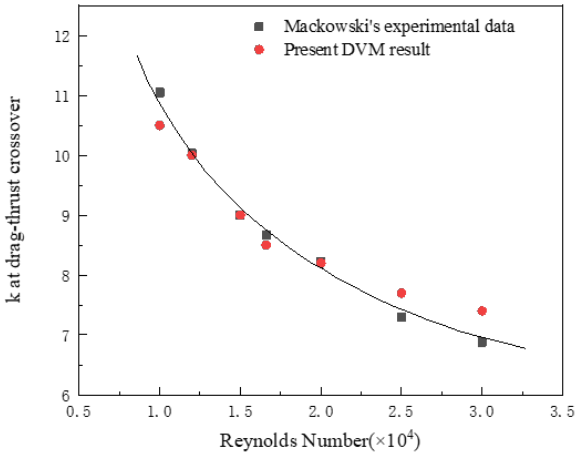

Figure 4. The crossover point of reduced frequency k at $\theta_0 = 2°$.

Under the condition of small pitching angles, the simulation can well predict the thrust coefficient results and its trend. However, as the angle increases, the simulation results of C_T present some gap compared with the experimental result. What's gratifying is that the simulation result can still predict the variation trend in the range of large angle amplitudes.

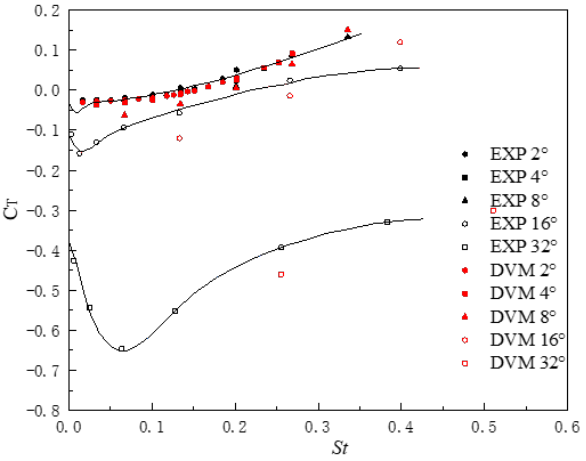

Figure 5. Mean thrust coefficient vs. Strouhal number St_A at different pitching angles when Re = 16600.

Figure 6 and Figure 7 present the oscillating amplitude of the unsteady thrust and lift coefficient in Mackowski and Williamson's experiment and the simulation of this paper at different pitching angles. It can be observed that the increase of the pitching angle and the frequency will lead to the increase of force coefficient, and this trend will be enhanced with the increase of pitching angles. Figure 6(b) and Figure 7(b) show the C_T/θ_0^2 and C_T/θ_0 amplitude, respectively. The scaling in C_T and C_Y work remarkably well across the whole range of pitching angles. The black lines shown are the prediction results of the linear theory introduced by Garrick [8]. It can be seen that across the whole range of pitching angles, the numerical calculation can well predict the value and variation trend of C_T and C_Y under different conditions. The oscillating amplitude of C_T/θ_0^2 and C_Y/θ_0 under all pitching angles can both be fitted into a curve, and the numerical calculation results can also reflect this feature.

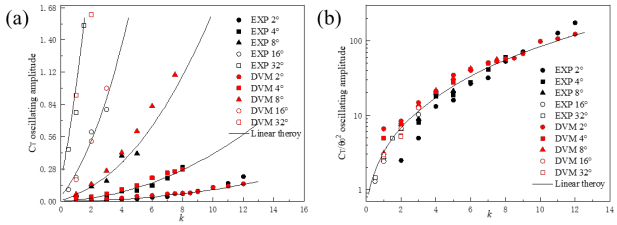

Figure 6. Amplitude of the varying component of the thrust coefficient at different pitching angles when Re = 16600: (**a**) C_T oscillating amplitude vs. reduced frequency k; (**b**) C_T oscillating amplitude divided by θ_0^2 vs. reduced frequency k.

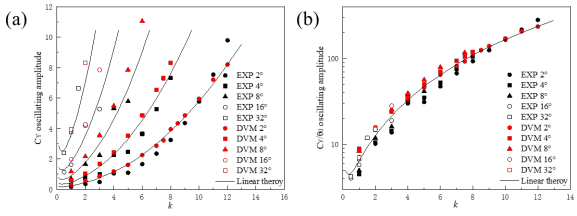

Figure 7. Amplitude of the varying component of the lift coefficient at different pitching angles when Re = 16600: (**a**) C_Y oscillating amplitude vs. reduced frequency k; (**b**) C_Y oscillating amplitude divided by θ_0 vs. reduced frequency k.

Figure 8 shows the spanwise vorticity results presented by Mackowski and Williamson's PIV measurements and the simulation result of this paper under the same conditions. It shows that no matter k = 2, k = 5 or k = 9, the simulation results present the consistent vorticity structure characteristics in the wake flow. As the reduced frequency k increases, the wake flow vortex mode changes from 4P + 2S to 2P and then to inverse-2S mode. Similar results can also be observed in Godoy-Diana et al. and Schnipper et al.'s research [11,12]. Figure 8 proves that the numerical calculation method introduced in this paper can not only predict the fluid force exerted on the body, but also can be used to obtain the wake structure of the pitching airfoil.

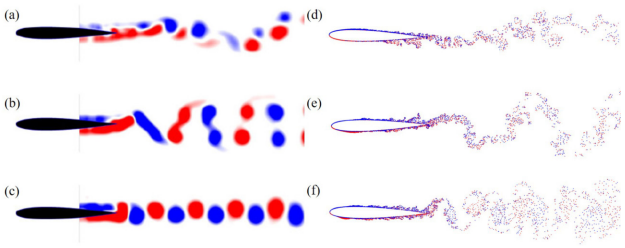

Figure 8. Spanwise vorticity presented by PIV measurements and DVM simulation with pitching angle $\theta_0 = 2°$, $Re = 16600$: (**a**) PIV measurement when $k = 2$; (**b**) PIV measurement when $k = 5$; (**c**) PIV measurement when $k = 9$; (**d**) simulation result when $k = 2$; (**e**) simulation result when $k = 5$; (**f**) simulation result when $k = 9$.

4. Conclusions

This study introduces a two-dimensional discrete vortex method to simulate the propulsive performance of the pitching airfoil. The vortices fall off randomly on the body surface instead of setting a fixed boundary layer thickness in advance. In addition, the vortex growing core method is used to simulate the viscous diffusion motion instead of the random walk method. By using this method, the pure pitching motion of the airfoil under the same configurations as Mackowski and Williamson's [25] experiment is simulated in order to verify the reliability of this method. The mechanical behavior and wake patterns with different flapping frequencies, amplitudes and Reynolds numbers are obtained and studied.

Under the condition of $Re = 12000$, $\theta_0 = 2°$, the mean value of the thrust coefficient C_T can be predicted well by the present numerical simulations. Within the increase of reduced frequency k, the x direction force acting on the airfoil will monotonically increase and complete the transition from drag to thrust. Similarly, the results of reduced frequency k when the transitions from drag to thrust occur under different Reynolds numbers also agree well with the experimental results. It can be observed that the crossover point which indicates the transitions from drag to thrust decreases monotonically with the increase of Reynolds number, indicating that it is easier to generate thrust for airfoils at higher Reynolds numbers. In the cases of different pitching angles, thrust results for small angle cases collapse reasonably well with Strouhal number. With larger pitching angles, there are some slight differences between the calculated lift coefficients and the experimental results, but it can still predict the amplitude and the variation trend of the force coefficient. Compared with PIV measurements, the simulation wake patterns visualized by the distribution of vortex elements present the consistent vorticity structure characteristics. It can be clearly observed that the transitions from the '4P + 2S' mode to the '2P' mode and eventually to the inverse '2S' mode occur gradually as the pitching frequency increases.

This study proves that the two-dimensional discrete vortex method introduced in this paper can be used to reasonably predict the propulsion performance and wake patterns on the pitching airfoil motion. As this paper mainly focuses on the validation of this method used in the pure pitching airfoil cases, further research can be also carried out to study the complex airfoil motion such as the heaving and pitching combined motion, based on the method introduced in this paper.

Author Contributions

Peng Ren: Conceptualization, Methodology, Validation, Investigation, Writing - Original Draft. Ke Lin: Investigation, Methodology, Writing-Review and Editing. Jiasong Wang: Conceptualization, Methodology, Resources, Writing-Review & Editing, Supervision, Funding acquisition.

Funding

This research was funded by Innovative Research Foundation of Ship General Performance #31422225.

Acknowledgement

The authors acknowledge the fund support from Innovative Research Foundation of Ship General Performance #31422225.

Data Availability

The data that support the findings of this study are available upon reasonable request.

Conflict of Interest

All authors disclosed no any conflict of interest.

References

[1] Jones, K.D., Bradshaw, C.J., Papadopoulos, J., et al., 2005. Bio-inspired design of flapping-wing micro air vehicles. The Aeronautical Journal. 109(1098), 385-393.

[2] Jones, K., Duggan, S., Platzer, M. (editors), 2001. Flapping-wing propulsion for a micro air vehicle. 39th Aerospace Sciences Meeting and Exhibit; 2001 Jan 8-11; Reno. p. 126.

[3] Read, D.A., Hover, F.S., Triantafyllou, M.S., 2003. Forces on oscillating foils for propulsion and maneuvering. Journal of Fluids and Structures. 17(1), 163-183.

[4] Cheng, Q., Liu, X., Ji, H.S., et al., 2017. Aerodynamic analysis of a helical vertical axis wind turbine. Energies. 10(4), 575.

[5] Lewthwaite, M.T., Amaechi, C.V., 2022. Numerical investigation of winglet aerodynamics and dimple effect of NACA 0017 airfoil for a freight aircraft. Inventions. 7(1), 31.

[6] Nguyen, M.T., Balduzzi, F., Goude, A., 2021. Effect of pitch angle on power and hydrodynamics of a vertical axis turbine. Ocean Engineering. 238, 109335.

[7] Von Karman, T., 1935. General aerodynamic theory-perfect fluids. Aerodynamic Theory. 2, 346-349.

[8] Garrick, I.E., 1936. Propulsion of a Flapping and Oscillating Airfoil [Internet]. Available from: https://ntrs.nasa.gov/api/citations/19930091642/downloads/19930091642.pdf

[9] Koochesfahani, M.M., 1989. Vortical patterns in the wake of an oscillating airfoil. AIAA Journal. 27(9), 1200-1205.

[10] Bohl, D.G., Koochesfahani, M.M., 2009. MTV measurements of the vortical field in the wake of an airfoil oscillating at high reduced frequency. Journal of Fluid Mechanics. 620, 63-88.

[11] Godoy-Diana, R., Aider, J.L., Wesfreid, J.E., 2008. Transitions in the wake of a flapping foil. Physical Review E. 77(1), 016308.

[12] Schnipper, T., Andersen, A., Bohr, T., 2009. Vortex wakes of a flapping foil. Journal of Fluid Mechanics. 633, 411-423.

[13] Young, J., Lai, J.C., 2004. Oscillation frequency and amplitude effects on the wake of a plunging airfoil. AIAA Journal. 42(10), 2042-2052.

[14] Chandravanshi, L.K., Chajjed, S., Sarkar, S. (editors), 2010. Study of wake pattern behind an oscillating airfoil. Proceeding of the 37th National & 4th International Conference on Fluid Mechanics and Fluid Power; 2010 Dec 16-18; Chennai. p. 16-18.

[15] Wu, Q., Huang, B., Wang, G., 2016. Lagrangian-based investigation of the transient flow structures around a pitching hydrofoil. Acta Mechanica Sinica. 32, 64-74.

[16] Lin, H., Vezza, M., Galbraith, R.M., 1997. Discrete vortex method for simulating unsteady flow. AIAA Journal. 35(3), 494-499.

[17] Sarkar, S., Venkatraman, K., 2006. Numerical simulation of thrust generating flow past a pitching airfoil. Computers & Fluids. 35(1), 16-42.

[18] Andersen, A., Bohr, T., Schnipper, T., et al., 2017. Wake structure and thrust generation of a flapping foil in two-dimensional flow. Journal of Fluid Mechanics. 812, R4.

[19] Priovolos, A.K., Filippas, E.S., Belibassakis, K.A., 2018. A vortex-based method for improved flexible flapping-foil thruster performance. Engineering Analysis with Boundary Elements. 95, 69-84.

[20] Chorin, A.J., 1973. Numerical study of slightly viscous flow. Journal of Fluid Mechanics. 57(4), 785-796.

[21] Yamamoto, C.T., Meneghini, J.R., Saltara, F., et al., 2004. Numerical simulations of vortex-induced vibration on flexible cylinders. Journal of Fluids and Structures. 19(4), 467-489.

[22] Meneghini, J.R., Saltara, F., de Andrade Fregonesi, R., et al., 2004. Numerical simulations of VIV on long flexible cylinders immersed in complex flow fields. European Journal of Mechanics-B/Fluids. 23(1), 51-63.

[23] Lin, K., Wang, J., 2019. Numerical simulation of vortex-induced vibration of long flexible risers using a SDVM-FEM coupled method. Ocean Engineering. 172, 468-486.

[24] Park, W.C., 1989. Computation of flow past single and multiple bluff bodies by a vortex tracking method [Ph.D. thesis]. Minneapolis: University of Minnesota.

[25] Mackowski, A.W., Williamson, C.H.K., 2015. Direct measurement of thrust and efficiency of an airfoil undergoing pure pitching. Journal of Fluid Mechanics. 765, 524-543.

[26] Qian, L., Vezza, M., 2001. A vorticity-based method for incompressible unsteady viscous flows. Journal of Computational Physics. 172(2), 515-542.

[27] Clarke, N.R., Tutty, O.R., 1994. Construction and validation of a discrete vortex method for the two-dimensional incompressible Navier-Stokes equations. Computers & Fluids. 23(6), 751-783.

[28] Wang, L., Yeung, R.W., 2016. Investigation of full and partial ground effects on a flapping foil hovering above a finite-sized platform. Physics of Fluids. 28(7).

[29] Walther, J.H., 1994. Discrete vortex method for two-dimensional flow past bodies of arbitrary shape undergoing prescribed rotary and translational motion. Den Polytekniske Læreanstalt: Lyngby.

[30] Spalart, P.R., 1983. Numerical simulation of separated flows. Stanford University: Stanford.

[31] Taylor, G.K., Nudds, R.L., Thomas, A.L., 2003. Flying and swimming animals cruise at a Strouhal number tuned for high power efficiency. Nature. 425(6959), 707-711.

[32] Laitone, E.V., 1997. Wind tunnel tests of wings at Reynolds numbers below 70 000. Experiments in Fluids. 23(5), 405-409.